Fascin-induced actin protrusions are suppressed by dendritic networks in giant unilamellar vesicles

Nadab H. Wubshet[a], Yashar Bashirzadeh[a], and Allen P. Liu[a,b,c,d,*]
[a]Department of Mechanical Engineering, [b]Department of Biomedical Engineering, [c]Cellular and Molecular Biology Program, and [d]Department of Biophysics, University of Michigan, Ann Arbor, MI, 48109

ABSTRACT The interactions between actin networks and cell membrane are immensely important for eukaryotic cell functions including cell shape changes, motility, polarity establishment, and adhesion. Actin-binding proteins are known to compete and cooperate using a finite amount of actin monomers to form distinct actin networks. How actin-bundling protein fascin and actin-branching protein Arp2/3 complex compete to remodel membranes is not entirely clear. To investigate fascin- and Arp2/3-mediated actin network remodeling, we applied a reconstitution approach encapsulating bundled and dendritic actin networks inside giant unilamellar vesicles (GUVs). Independently reconstituted, membrane-bound Arp2/3 nucleation forms an actin cortex in GUVs, whereas fascin mediates formation of actin bundles that protrude out of GUVs. Coencapsulating both fascin and Arp2/3 complex leads to polarized dendritic aggregates and significantly reduces membrane protrusions, irrespective of whether the dendritic network is membrane bound or not. However, reducing Arp2/3 complex while increasing fascin restores membrane protrusion. Such changes in network assembly and the subsequent interplay with membrane can be attributed to competition between fascin and Arp2/3 complex to utilize a finite pool of actin.

INTRODUCTION

Membrane remodeling due to assembly and disassembly of the actin cytoskeleton is critical to many cellular processes, including cell migration, cell division, and endocytosis (Schafer, 2002; Farsad and De Camilli, 2003). The ability for actin cytoskeleton to provide structural functionalities in processes like cell movement, adhesion, polarity, and molecular transport depends on the spatial and temporal dynamics of actin networks and the magnitude and direction of forces exerted by these networks (Schmidt and Hall, 1998; Fletcher and Mullins, 2010). These dynamic changes in actin networks are achieved by actin-binding proteins which enable self-organization of diverse types of actin networks within a confined and shared space while utilizing a limited amount of actin monomers (Bashirzadeh and Liu, 2019; Kadzik et al., 2020). Inside the cell, multiple actin-binding proteins compete and collaborate to construct functional actin architectures (Kadzik et al., 2020). For example, filopodia formed by bundled actin filaments and lamellipodia formed by Arp2/3-branched networks can be found at the leading edge of a motile cell (Welch, 1999; Vignjevic et al., 2006). Similarly, alpha-actinin is prevalent at focal points between cell-to-cell or cell-to-substrate contacts facilitating cell adhesion (Otey et al., 1990; Knudsen et al., 1995). Moreover, formin, profilin, cofilin, and capping proteins are responsible for regulating actin polymerization and depolymerization. With the aid of numerous actin-binding proteins, actin networks actively and dynamically remodel the cell membrane.

Fascin and Arp2/3 complex are among the well-studied actin-binding proteins that are found in protrusive structures at the cell membrane. Fascin is a 55-kDa short actin cross-linker that bundles actin filaments in a tightly packed and parallel manner (Vignjevic et al., 2006). Fascin-bundled actin networks are responsible for fingerlike protrusions in structures like filopodia and microspikes. These cellular structures mediate cell movement and cell–cell interaction

(Adams, 2004; Vignjevic et al., 2006). Arp2/3 complex, on the other hand, is a 224-kDa multifunctional actin-branching protein made up of seven subunits (Robinson et al., 2001). Arp2/3 complex, when activated by the VCA domain of the neural Wiskott-Aldrich syndrome protein (N-WASp) (Higgs and Pollard, 1999; Weaver et al., 2002), branches actin filaments to form a dendritic network that plays a major role in force generation at the leading edge of a cell to mediate cell motility (Robinson et al., 2001; Goley and Welch, 2006). To study the roles of these actin-binding proteins, in vitro reconstitution and studies in cells have defined the roles of fascin in filopodia formation and cell migration (Vignjevic et al., 2003, 2006; Adams, 2004; Haviv et al., 2006; Ideses et al., 2008; Machesky and Li, 2010), as well as the role of Arp2/3 complex in the formation of an actin cortex (Mullins et al., 1998; Pollard and Beltzner, 2002; Pollard, 2007; Pontani et al., 2009; Carvalho et al., 2013). As an alternative experimental system, others have biochemically reconstituted actin networks on the outside surface or inside giant unilamellar vesicles (GUVs) to independently study actin networks formed by fascin and Arp2/3 complex and their respective interaction with lipid membranes. For example, when encapsulated inside a GUV, fascin was shown to form actin bundles which induced reversible membrane protrusions or formed contractile rings (Tsai and Koenderink, 2015; Bashirzadeh et al., 2020b; Litschel et al., 2021). When polymerized on the outside, reconstitution of an Arp2/3-branched network led to the emergence of short filopodium-like actin protrusions into the GUV lumen in the absence of fascin (Liu et al., 2008; Simon et al., 2019).

Considering the strong evidence that fascin and Arp2/3 complex organize different types of actin networks in cells, it was surprising that in vitro reconstitution studies of branched networks on GUVs formed filopodium-like protrusions. Thus, it is critical to investigate how these two actin-binding proteins might cooperate to organize actin networks and thereby remodel the membrane. Coencapsulation of multiple actin-binding proteins in previous studies have revealed formation of emergent structures as a result of either synergy or competition between different actin-binding proteins. It was shown recently that the coencapsulation of α-actinin together with fascin impairs the formation of protrusive bundled actin structures (Bashirzadeh et al., 2020b). Similarly, others have shown that membrane remodeling caused by an Arp2/3-induced actin cortex can be tuned by changing the concentration of capping protein (Dürre et al., 2018). In an attempt to show the transformation of lamellipodia into filopodia, a membrane-free assay reconstituting actin networks formed by fascin and Arp2/3 complex revealed a transition from an aster-like actin network, which occurred as a result of Arp2/3-mediated nucleation, to star-like networks due to fascin-mediated bundling (Haviv et al., 2006; Ideses et al., 2008). Finally, a previous reconstitution study has shown that fascin-bundled actin can drive motility in Listeria independent of Arp2/3-dependent motility in a system that has both fascin and Arp2/3 complex (Brieher et al., 2004). Although these are significant findings, these prior studies have not considered the interaction of actin networks formed by fascin bundling and Arp2/3 nucleation with membrane. To our knowledge, there have been no studies that investigated the interplay between fascin-bundled and Arp2/3-branched networks in a confined membrane-bound space.
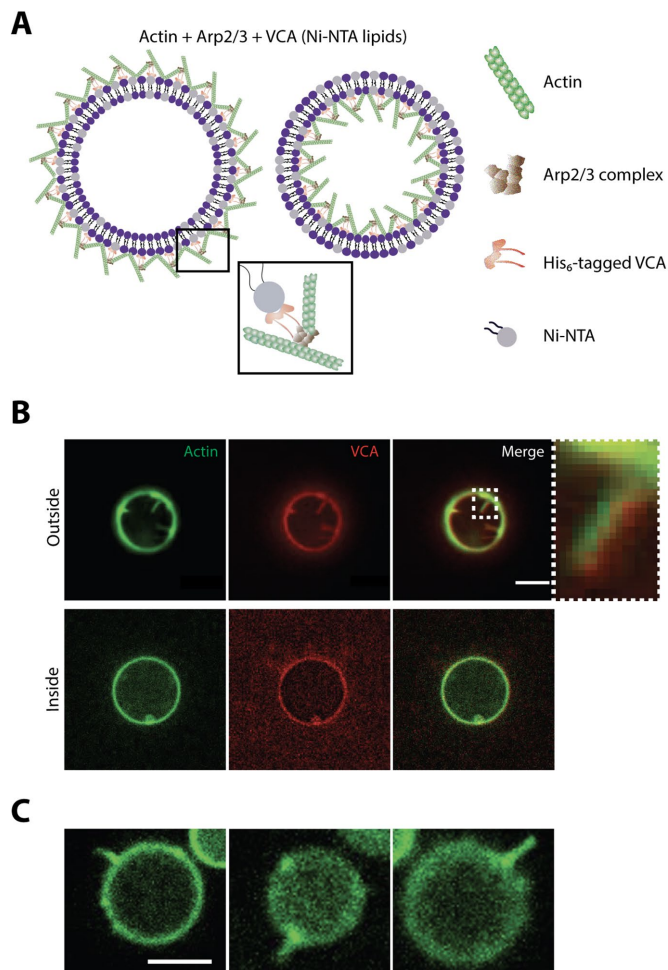
In this work, we study the interaction between actin networks formed by fascin and Arp2/3 complex inside GUVs. We hypothesize that these actin-binding proteins compete for actin and would alter the resulting networks and consequently affect membrane remodeling. We compare this composite network system with known benchmark systems generated by encapsulating actin with fascin or Arp2/3 complex alone. We show that the Arp2/3-branched network

at the membrane forms a uniform cortex, while the fascin-bundled network induces protrusions in a fascin concentration-dependent manner. Our experiments show that coencapsulation of the fascin and Arp2/3 complex results in the inhibition of actin bundle protrusions and shortens the bundle lengths compared with a fascin-only condition. Our results suggest that dendritic network formation can suppress filopodia formation through an actin monomer competition mechanism.

RESULTS AND DISCUSSION

We first implemented two approaches to assemble a minimal actin cortex by nucleating actin at the membrane using His$_6$-tagged VCA of N-WASp to activate Arp2/3 complex. The first approach is similar to previous studies reported by Liu et al (Liu and Fletcher, 2006; Liu et al., 2008), in which dendritic actin networks are polymerized on the external leaflet of the GUV membrane. In this work, we used an emulsion-transfer method called continuous droplet interface crossing encapsulation (cDICE) that is adopted to a benchtop centrifuge to generate GUVs of a variety of sizes, with a composition of DOPC/cholesterol/DGS-Ni-NTA (70/25/5). To form an actin cortex on the surface of GUVs, we used an outer solution comprising 5.3 μM actin, 1 μM Arp2/3, 0.5 μM His$_6$-tagged VCA in actin polymerization buffer for cDICE. With this approach, His$_6$-tagged VCA binds to Ni-NTA lipids due to the metal affinity to the His$_6$-tag, thereby localizing the activation of Arp2/3 complex at the outer leaflet of the membrane (Figure 1A). Similar to previous observations by us and others (Liu et al., 2008; Simon et al., 2019), we observed a uniform, Arp2/3-nucleated, actin cortex with thin actin protrusions projecting into the vesicle lumen (Figure 1B; Supplemental Movie S1). In our second approach, we encapsulated the same proteins at the same concentrations inside the GUV instead. In contrast, we observed a uniform actin cortex but without any formation of thin actin protrusions (Figure 1B; Supplemental Figure S1A). The addition of capping protein CapZ to regulate actin filament lengths did not alter the actin cortex in GUVs (Supplemental Figure S1B). It was not immediately clear as to why nucleating dendritic network assembly on the inner leaflet of the membrane did not generate inside-out protrusions. We suspected that this could be a result of differences in membrane curvature with respect to the direction of protrusion, where the force for the actin bundle to push and deform from the outside is lower than the force required to protrude the membrane from the inside from a force balance analysis—membrane tension would help with outside-in protrusions but would inhibit inside-out protrusions. The energetics of out-tube versus in-tube have also been described to show that out-tube has higher energetics compared with in-tube. Given these considerations, we hypothesize that lowering membrane tension may allow the formation of inside-out protrusions (Lipowsky, 2014). To test this, we lowered membrane tension by deflating vesicles using a hyperosmotic solution of 70 mOsm difference and observed membrane protrusions induced by actin cortex from the inside (Figure 1C).

After demonstrating that we can form a dendritic network, we next sought to investigate how Arp2/3 activation might influence a fascin-bundled network. For this, we compared an encapsulated fascin-bundled network known to deform membranes with and without nonmembrane-bound dendritic actin networks (Figure 2A), which can be achieved by leaving out Ni-NTA lipids. We encapsulated fascin and actin at three different fascin-to-actin ratios of 1:2 (2.65 μM fascin), 1:10, and 1:20 in actin polymerization buffer in GUVs. At a high fascin concentration, we found that fascin-bundled actin frequently deformed the GUV membrane and GUV deformation reduced with decreasing fascin concentration from ~85% to ~60% of GUVs over 10 μm in diameter (Figure 2, B and C). This indicates that

A Actin + Arp2/3 + VCA (Ni-NTA lipids)

Actin

Arp2/3 complex

His6-tagged VCA

Ni-NTA

B

Outside — Actin | VCA | Merge

Inside

C

FIGURE 1: Actin cortex reconstitution. (A) Schematic representation of two different approaches of actin cortex reconstitution. Actin cortex reconstitution from the outside (left) or inside (right) of GUVs by via activation of Arp2/3 complex using His6-tagged VCA bound to Ni-NTA lipids. (B) Representative confocal fluorescence images showing dendritic actin cortex (actin: 5.3 μM; Arp2/3 complex: 1 μM; His6-tagged VCA: 0.5 μM) networks on the outer leaflet of the GUVs (top) or on the inner leaflet (bottom). Actin protrusions can be seen in GUV lumen (inset on top right). GUVs with a composition of 70/25/5 DOPC/cholesterol/DGS Ni-NTA are made by cDICE. Scale bar is 10 μm. (C) Representative confocal fluorescence images showing dendritic actin cortex (actin: 5.3 μM; Arp2/3 complex: 1 μM; His6-tagged VCA: 0.5 μM) networks on the inner leaflet of the GUVs of a hyperosmotic condition with a difference of 70 mOsm between inner and outer solution.

elongation of stiff fascin-bundled actin is the driving force of GUV deformation. Inclusion of CapZ prevented the formation of long actin bundles and abrogated membrane deformation (Supplemental Figure S1B). By comparison, in the presence of an Arp2/3-nucleated dendritic network, the appearance of bundled actin diminished and GUV deformation was significantly reduced to less than 10% (Figure 2B,C). Since fascin and Arp2/3 complex compete for the same pool of actin inside GUVs, we expected bundle length to change when Arp2/3 complex was added. From 3D reconstructed image stacks, we skeletonized actin networks and quantified bundle lengths. From this analysis, as one would expect, we found that there was a significant decrease in the bundle length with decreasing fascin that coincided with a reduction of GUV deformation probability (Figure 2D).

More importantly, the formation of dendritic network drastically reduced actin bundle lengths for the two high fascin concentrations (Figure 2D). Our finding is in accord with previous findings (Haviv et al., 2006; Ideses et al., 2008) where bulk experiments showed that an increase in the concentration of fascin results in an increase in actin bundle length during coassembly of actin networks by fascin and Arp2/3 complex. Consistent with this, we quantified the number of branch nodes in each reaction condition and found that there was an increase in branching of bundles when Arp2/3 complex was added (Supplemental Figure S2). Together, these observations support the idea that both fascin and Arp2/3 complex simultaneously compete for the limited pool of actin and thus leading to the inhibition of fascin-bundled actin protrusions that are otherwise prevalent when fascin is encapsulated alone with actin. It is worth pointing out that all reconstituted systems, whether bulk or confined, have finite amounts of proteins. In a confined system such as GUVs with a size of tens of microns, the pool of actin and actin-binding proteins available is very different compared with a reconstitution system with polystyrene beads as the nucleating surface, even though such a bulk system also has a finite pool of proteins.

Since a lumenal dendritic network strongly suppressed fascin-bunded network formation and the resultant GUV deformation, we wonder if a membrane-bound dendritic network would have the same effect on bundled network formation. To test this, we encapsulated the same concentrations of Arp2/3 complex, His6-tagged VCA, actin, and fascin used in the earlier experiment in actin polymerization buffer in Ni-NTA-containing GUVs. In contrast to the uniform actin cortex that we reported in Figure 1B when there is no fascin, we observed distinct network phenotypes that can be categorized into two major groups (Figure 3A). The first and most common structure appearing in more than 80% of the GUVs is polarization of membrane-bound dendritic actin aggregates (Supplemental Movie S2). The second category, at about 20% of GUVs, had a cortex-like structure similar to GUVs with membrane-bound dendritic networks but without fascin added. We observed membrane-associated nonprotruding bundles extending toward the lumen; this can occur with both polarized dendritic aggregates and cortex-like networks. Under this condition, we rarely saw GUV deformation.

Since it was clear now that dendritic and bundle network 'compete' in a confined environment, we asked whether reducing the amount of dendritic network might rescue GUV deformation by bundled actin. We fixed the concentrations of all proteins and varied the concentration of Arp2/3 complex from 2 μM to 500 nM and quantified the fraction of GUVs that exhibited membrane protrusion. With decreasing Arp2/3 complex concentration, we observed a decrease in cortex formation concomitant with an increase in bundle formation at the membrane (Figure 3B); interestingly, this resulted in an increase in protrusion probability from ~2% to ~20% (Figure 3C). This indicates that, although there is membrane binding of the dendritic network, the impact of fascin is more prevalent at lower concentrations of Arp2/3 complex due to decreased competition for finite actin inside the GUVs. To further illustrate this, when we increased fascin concentration in the presence of membrane-bound dendritic networks, we observed a reduction of polarized dendritic aggregates and a concomitant increase of actin bundles (Figure 3B). These bundles were longer, straight, and protrusive, reminiscent of fascin-bundled actin networks shown in Figure 2B. Consequently, the fraction of GUVs with protrusions increased to ~50% (Figure 3C). Altogether, these results support the idea that protrusions by bundled actin can be suppressed by dendritic actin networks, but a membrane-bound dendritic network can actually give rise to membrane deformation in the presence of fascin.
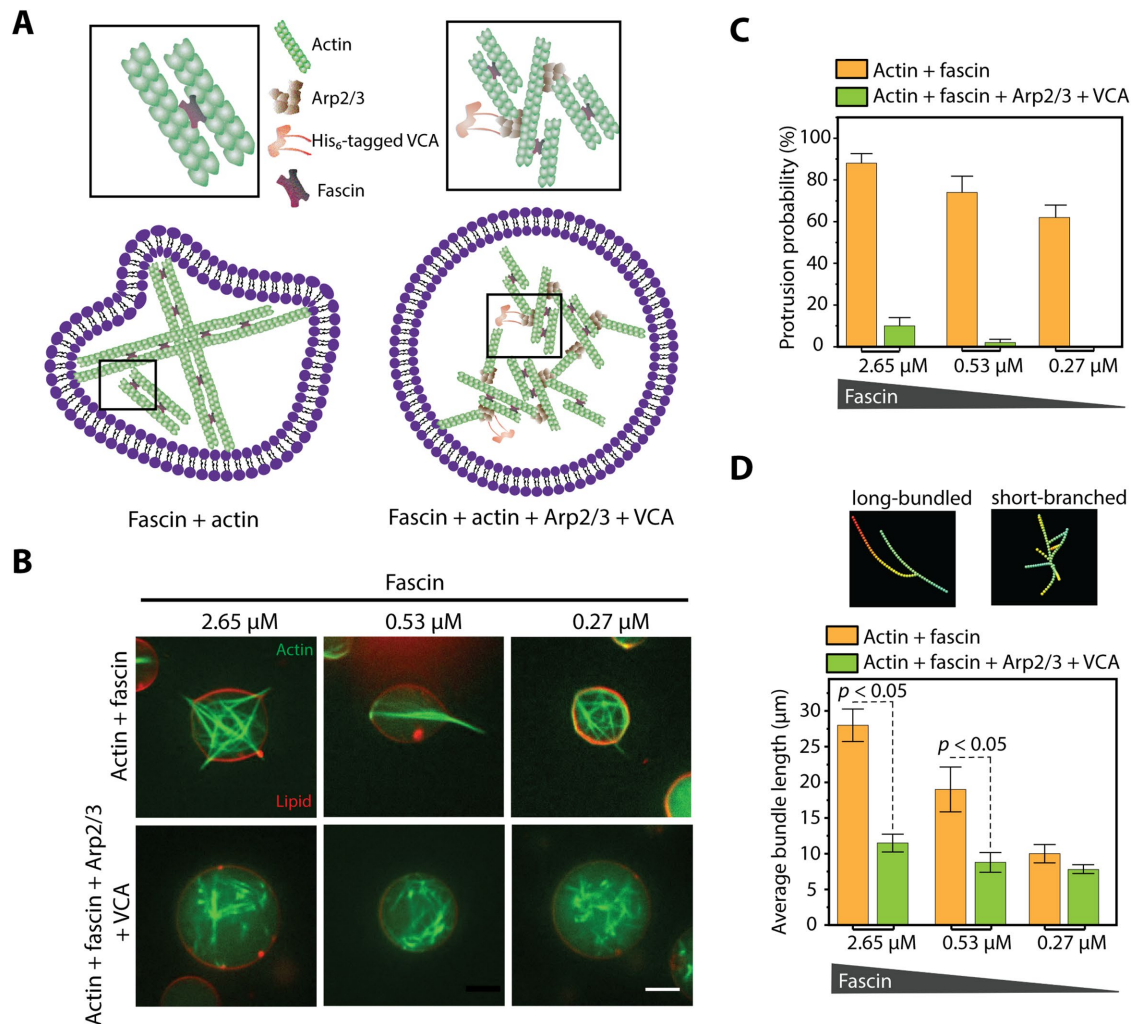
FIGURE 2: Coencapsulation of fascin and Arp2/3 complex not bound to membrane. (A) Schematic representation of actin bundles formed by fascin inside a GUV (left) and network formation by coencapsulation of fascin with activated Arp2/3 complex not bound to the membrane (right). (B) Representative confocal fluorescence images of fascin-actin networks (5.3 µM actin) without (top) or with (bottom) Arp2/3 complex as a function of fascin concentration as indicated. In the cases where Arp2/3 complex was added, the concentrations of actin (5.3 µM), His$_6$-tagged VCA (0.5 µM), and Arp2/3 complex (1 µM) were kept constant for all three fascin concentrations. GUVs had a composition of 70/30 DOPC/cholesterol. Scale bar is 10 µm. (C) The probability of protrusion formation for experimental conditions as indicated in (B). $N > 25$ for ≥ 2 replicates per category. Error bars denote counting error assuming a binomial distribution. (D) Length of actin bundles measured from 3D skeletonized filaments under different conditions shown in (B). Examples of what the traced bundles look like are shown. N > 25 for ≥2 replicates per category. Error bars represent standard error of the mean.

To further illustrate the role of competition for available actin monomers, we encapsulated the same concentrations of Arp2/3 complex, His$_6$-tagged VCA, and fascin while varying the concentration of actin at 2.65 µM (half of previous concentration) and 10.6 µM (double the previous concentration). As shown in Figure 3B, the activity of fascin was suppressed at a low actin concentration resulting in predominantly uniform cortex and no protrusions were observed (Figure 3C), while a high actin concentration resulted in membrane-associated and polarized actin bundles. Ideses *et al.* (2008) and Brill-Karniely *et al.* (2009) describe that an increase in the length of individual actin filaments lowers the bending energy required to bring them to close proximity and transform them to thicker bundles through binding of fascin. This in in accord with our finding as increased concentration of actin facilitates the formation of longer filaments, subsequently resulting in fascin-bundled actin.

In summary, our work examined the interplay between dendritic and bundled actin networks by reconstituting them inside GUVs. We compared actin networks assembled by the coencapsulating fascin and Arp2/3 complex to actin networks assembled by encapsulating either of these actin-binding proteins alone. Fascin is a short cross-linker that cross-links actin filaments into parallel and tight bundles. Depending on the concentration of fascin and the size confinement space, fascin is known to induce membrane protrusions (Tsai and Koenderink, 2015; Bashirzadeh *et al.*, 2020b), whereas membrane-bound activation of Arp2/3 complex nucleates actin to form a dendritic cortex (Liu *et al.*, 2008). Consistent with prior work (Liu *et al.*, 2008), reconstitution of a dendritic actin cortex on the external membrane leaflet results in membrane protrusions directed toward the GUV lumen. Interestingly, internally reconstituted dendritic cortex results in a uniform distribution of
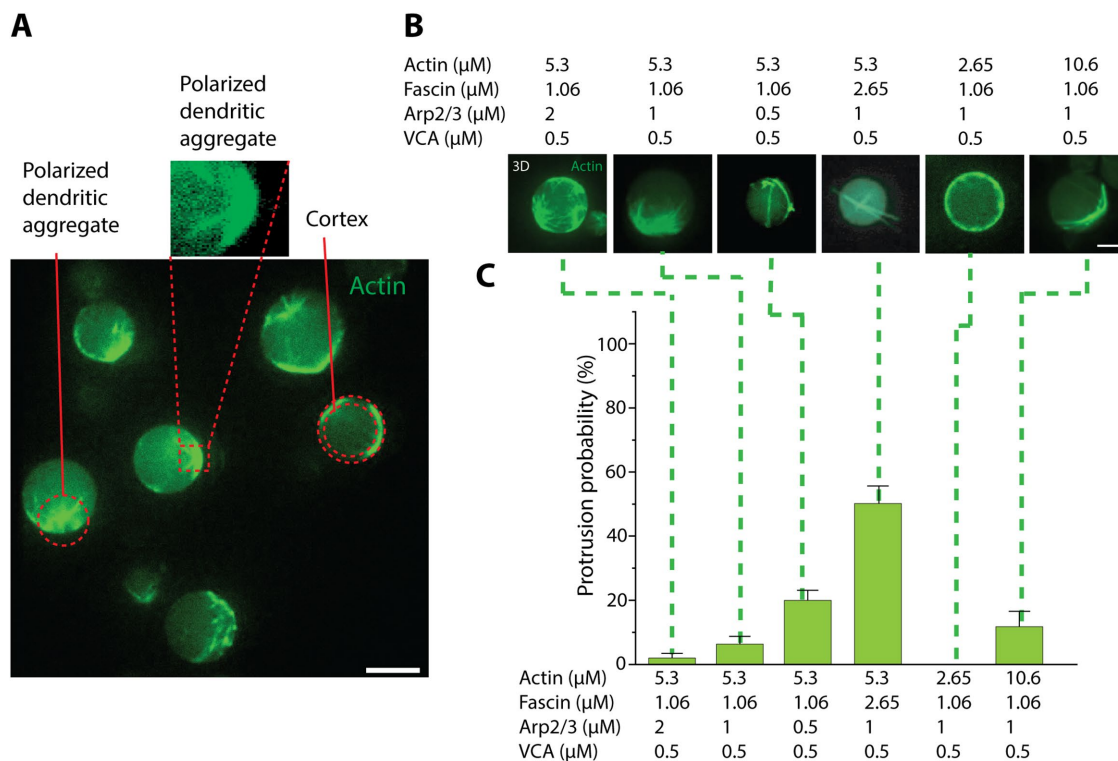
FIGURE 3: Coencapsulation of fascin and membrane-bound Arp2/3 complex. (A) A representative confocal fluorescence image showing distinct actin network structures by coencapsulation of actin (5.3 µM), fascin (0.53 µM), and Arp2/3 complex (1 µM). Arp2/3 complex is activated by His$_6$-tagged VCA (0.5 µM) bound to the inner leaflet of the GUVs in the presence of 5% Ni-NTA lipid. (B) Representative confocal fluorescence images of actin networks inside single GUVs at different concentrations of actin, fascin, Arp2/3 complex, and His$_6$-tagged VCA as indicated. Scale bar is 10 µm. (C) Protrusion probability for each experimental condition as indicated and corresponding to images in (B). $N > 25$ for ≥ 2 replicates per category. Error bars denote counting error assuming a binomial distribution.

membrane-nucleated actin with no protrusions, and this has also been observed in a prior study using a different approach to activate Arp2/3 complex at the membrane (Pontani et al., 2009). Localized deformations in the form of small changes in membrane curvature have been shown when reconstituting Arp2/3-nucleated cortex with regulated capping protein inside a GUV (Dürre et al., 2018), yet no membrane protrusions were observed. The different outcomes from nucleating dendritic actin between outside and inside GUVs could be due to the curvature; from the outside, actin network is convex to the membrane, whereas from the inside, actin network is concave to the membrane. In the convex case, the direction of actin protrusive force is in the same direction of membrane tension and thus making protrusion possible. Simon et al. reported that actin protrusions on GUVs can be tuned by membrane tension (Simon et al., 2019), and our experiments show that lowering membrane tension results in the emergence of protrusive actin structures from dendritic networks can be reconstituted from inside GUVs.

By coencapsulating fascin and Arp2/3 complex, our results revealed that dendritic network formed in the GUV lumen suppresses the assembly of protrusive fascin-bundles by shortening bundle length and possibly by increasing branching of actin filaments, thereby stunting bundle growth. When the dendritic networks were assembled at the GUV membrane instead, we found an emergence of polarized dendritic aggregates with membrane-associated bundles. It was not immediately clear as to why polarized aggregation of networks were prevalent; however, similar nonhomogeneity in actin cortex has been shown with increasing cross-linker concentra-

tion (Maciver et al., 1991; Tan et al., 2018). Reconstituted inside water-in-oil droplets, Tan et al. (2018) showed the transition from a uniformly distributed Arp2/3-nucleated actomyosin cortex into asymmetrically aggregated cortex by increasing the concentration of α-actinin. In the case of encapsulating fascin and membrane-activated Arp2/3 complex, we show that formation of polarized dendritic aggregates is common. Moreover, decreasing the concentration of Arp2/3 complex and increasing the concentration of fascin result in higher protrusion probability. This finding may have implications consistent with the convergent elongation model for filopodia initiation in cells, which posits the transition from a lamellipodia to a filopodia by reorganization of the dendritic network to initiate fascin-mediated actin bundling (Svitkina et al., 2003). To conclude, we speculate that the inhibition of actin bundle-induced membrane protrusions is due to competition for finite actin available inside the vesicles. This finding would be distinct in our experimental system compared with previous studies that did not have confinement. Distinct actin network architectures due to competing actin cross-linkers have been observed by reconstituting fascin and α-actinin (Bashirzadeh et al., 2020a). The precise mechanism by which protrusions are inhibited and how cortex aggregation is formed is still open for investigation. Future work can potentially dissect the dynamics of actin cross-linkers altering a uniform cortex into asymmetric aggregates.

MATERIALS AND METHOD
Request a protocol through *Bio-protocol*.

Preparation of proteins

We purified actin from rabbit skeletal muscle acetone powder (Pel-Freez Biologicals) as described previously (Pardee and Aspudich, 1982) or purchased it from Cytoskeleton Inc. (USA). ATTO 488 actin and CapZ were purchased from Hypermol (Germany). α-Actinin from rabbit skeletal muscle and Arp2/3 complex from porcine brain were purchased from Cytoskeleton Inc. We purified human fascin from *Escherichia coli* as glutathione-S-transferase (GST) fusion protein (Vignjevic *et al.*, 2003). For purification, BL21(DE3) *E. coli* cells were transformed with pGEX-4T-3 (GE Healthcare) containing the coding sequences of fascin. Cells were grown at 37°C while shaking at 220 rpm until the OD_{600} reached 0.5–0.6. Protein expression was induced with 0.1 mM IPTG and cell culture was incubated at 24°C for 8 h. Cells were harvested by centrifugation at $4000 \times g$ for 15 min and washed with phosphate-buffered saline (PBS) once. Pellets were stored at –80°C until the day of purification. Cell pellets were resuspended in lysis buffer (20 mM K-HEPES, pH 7.5, 100 mM NaCl, 1 mM EDTA, 1 mM phenylmethylsulfonyl fluoride [PMSF]) and ruptured by sonication. Cell lysates were centrifuged at $75,000 \times g$ for 25 min and supernatants were loaded on a GSTrap FF 1-ml column (GE Healthcare) using an AKTA Start purification system (GE Healthcare) at a flow rate of 1 ml/min. The column was washed with 15 ml washing buffer (20 mM K-HEPES pH 7.5, 100 mM NaCl) and the protein was eluted with 5 ml elution buffer (washing buffer + 10 mM reduced L-glutathione). Purified fascin was dialyzed against 1 L of PBS twice for 3 h and once overnight at 4°C. Protein concentration was calculated by UV absorption using predicted molar extinction coefficients (ExPasy) of 110,700 $M^{-1}cm^{-1}$. Proteins were concentrated with Centricon filters (Merck-Millipore) when needed and/or diluted to a final concentration of 1 mg/ml in PBS.

We purified hexa-histidine-tagged VCA (His$_6$-tagged VCA) domain from N-WASp following the same steps by transformation of BL21(DE3) RIL *E. coli with plasmids* containing the coding sequences of VCA. Induction was performed using 0.5 mM IPTG and incubation of cells at 37°C for 3 h. Cells were harvested by centrifugation at 5000 rpm for 10 min and resuspended in lysis buffer containing 20 mM HEPES, pH 7.5, 200 mM NaCl, 10 mM imidazole, and 1 mg/ml lysozyme. Lysate was then flash-frozen with liquid nitrogen. Cells were thawed, followed by the addition of 1 mM PMSF, and then lysed by sonication. The lysate was incubated with Ni-NTA resin (600 µl resin for 2 ml of lysates) for 2.5 h, washed several times with 20 mM HEPES, pH 7.5 containing 200 mM NaCl, and eluted in elution buffer (20 mM HEPES, pH 7.5, 200 mM NaCl, 250 mM imidazole) from a column into aliquots. Fractions containing purified His$_6$-VCA were dialyzed in 20 mM HEPES, pH 7.5, 200 mM NaCl, 1 mM TCEP overnight. The concentration of VCA was determined using Nanodrop (Thermo Fisher Scientific).

Production of GUVs

All lipids were purchased from Avanti Polar Lipids (Alabaster, AL). We modified cDICE technique for robust encapsulation in GUVs of various sizes as previously reported (Bashirzadeh *et al.*, 2020b). Briefly, a custom 3D-printed chamber is mounted on a benchtop stir plate and rotated at 1200 rpm. An outer solution of 200 mM glucose (matched to the osmolarity of the inner solution) is pipetted into the chamber. Then, the lipid mixture (70% DOPC, 25% cholesterol, 5% DGS-NTA[Ni]) in a mixture of silicone oil and mineral oil (4:1) is added. The lipid–oil solution forms an interface with the outer solution; 20 µl inner solution containing 7.5% OptiPrep (a solution that increases the density of inner solution encapsulated inside GUVs so that they can settle at the bottom of the imaging chamber [Bashirzadeh *et al.*, 2020b; Litschel *et al.*, 2021]) was added into

700 µl of the lipid–oil mix, and droplets were generated by pipetting up and down. For reconstitution of confined actin networks, the inner solution contained 5.3 µM actin including 10% ATTO 488 actin in polymerization buffer, 7.5% OptiPrep, 0–2.65 µM fascin, 0–2 µM Arp2/3 complex, and 0.5 µM His$_6$-VCA as indicated. We also encapsulated 200 nM capping protein (CapZ) to regulate actin filament lengths inside vesicles. GUVs were then generated by dispensing the droplets into the cDICE chamber. A lipid bilayer is formed when a second layer of lipid is acquired as the droplets cross the lipid–oil outer solution interface. In the case of branched actin networks, reconstituted on the outer surface of GUVs, vesicles were made using 200 mM glucose for both inner and outer solution. GUVs were then collected and incubated in 5.3 µM actin including 10% ATTO 488 actin, 1 µM Arp2/3 complex, and 0.5 µM His$_6$-VCA and actin polymerization buffer (50 mM KCl, 2 mM MgCl$_2$, 0.2 mM CaCl$_2$, and 4.2 mM ATP in 15 mM Tris, pH 7.5).

Imaging and image processing

Following cDICE, GUVs were transferred to a 96-well plate for imaging. OptiPrep in the inner solution increases GUV density and accelerates sedimentation of GUVs onto the bottom of the well plate. An Olympus IX-81 inverted microscope equipped with a spinning disk confocal (Yokogawa CSU-X1), AOTF-controlled solid-state lasers (Andor Technology), and an iXON3 EMCCD camera (Andor Technology) were used for microscopy and controlled by using MetaMorph software (Molecular Devices). Images were acquired by using an oil immersion 60×/1.4 NA objective lens. Fluorescence images of actin and lipids were taken with 488- and 561-nm laser excitation, respectively. Z-stack fluorescence confocal image sequence of lipids and actin was taken with a z-step size of 0.5 µm.

Images were processed using ImageJ/Fiji (Schindelin *et al.*, 2012; Schneider *et al.*, 2012; Litschel *et al.*, 2021), SOAX (Xu *et al.*, 2014, 2015), and MATLAB routines (Bashirzadeh *et al.*, 2020a). For 3D characterization of actin bundle structures, we generated skeletonized models from regions of interest in actin images. To optimize the images for identification of actin bundles, images were first preprocessed using ImageJ/Fiji. The structures from z-stack images are identified and extracted with SOAX source code (Xu *et al.*, 2014, 2015) by active contour methods. SOAX program stores all the coordinates of snakes (skeletonized bundles) and joints in a .txt file. Custom MATLAB routines were written to reconstruct the text as a Chimera marker file, include a colormap of z coordinates, and save the file as .cmm format. This process enables UCSF Chimera (Pettersen *et al.*, 2004) to read the file and provide a better 3D visualization of actin structures for selecting actin bundles and measuring parameters such as bundle length using MATLAB.

Data analysis

Actin bundle phenotypes and GUV deformation were characterized from z-stack actin and lipid images by counting the number of GUVs that do not assume a spherical shape and are deformed by actin bundles. The diameter of a GUV was measured by line scan from GUV images. The percentages and probabilities of GUV shape changes were obtained by their count divided by the total number of GUVs with actin bundles (i.e., GUVs encapsulating fluorescent actin monomers with no sign of bundling activity were not counted). We calculated the length of actin bundles using the skeletonized images of actin bundles. Bundle length values are shown as average ± standard error of the mean of the data at each fascin concentration.

For probability and percentage measurements, at least two independent experiments were conducted for each condition indicated.

Error bars for reporting protrusion probability represent counting error. Assuming a binomial distribution, this error is calculated as $\sqrt{prob(1-prob)/N}$', where $prob$ is the probability of an observation and N is the total number of observations. The reported p values are two-tailed, unpaired two-sample Student's t test assuming unequal variances.

REFERENCES

Adams JC (2004). Roles of fascin in cell adhesion and motility. Curr Opin Cell Biol 16, 590–596.

Bashirzadeh Y, Liu AP (2019). Encapsulation of the cytoskeleton: towards mimicking the mechanics of a cell. Soft Matter 15, 8425–8436.

Bashirzadeh Y, Redford SA, Lorpaiboon C, Groaz A, Litschel T, Schwille P, Hocky GM, Dinner AR, Liu AP (2020a). Actin crosslinker competition and sorting drive emergent GUV size-dependent actin network architecture. BioRxiv, https://doi.org/10.1101/2020.10.03.322354.

Bashirzadeh Y, Wubshet NH, Liu AP (2020b). Confinement geometry tunes fascin-actin bundle structures and consequently the shape of a lipid bilayer vesicle. Front Mol Biosci 7, 610277.

Brieher WM, Coughlin M, Mitchison TJ (2004). Fascin-mediated propulsion of Listeria monocytogenes independent of frequent nucleation by the Arp2/3 complex. J Cell Biol 165, 233–242.

Brill-Karniely Y, Ideses Y, Bernheim-Groswasser A, Ben-Shaul A (2009). From branched networks of actin filaments to bundles. ChemPhysChem 10, 2818–2827.

Carvalho K, Lemière J, Faqir F, Manzi J, Blanchoin L, Plastino J, Betz T, Sykes C (2013). Actin polymerization or myosin contraction: two ways to build up cortical tension for symmetry breaking. Philos Trans R Soc B Biol Sci 368, 20130005.

Dürre K, Keber FC, Bleicher P, Brauns F, Cyron CJ, Faix J, Bausch AR (2018). Capping protein-controlled actin polymerization shapes lipid membranes. Nat Commun 9, 1–11.

Farsad K, De Camilli P (2003). Mechanisms of membrane deformation. Curr Opin Cell Biol 15, 372–381.

Fletcher DA, Mullins RD (2010). Cell mechanics and the cytoskeleton. Nature 463, 485–492.

Goley ED, Welch MD (2006). The ARP2/3 complex: an actin nucleator comes of age. Nat Rev Mol Cell Biol 7, 713–726.

Haviv L, Brill-Karniely Y, Mahaffy R, Backouche F, Ben-Shaul A, Pollard TD, Bernheim-Groswasser A (2006). Reconstitution of the transition from lamellipodium to filopodium in a membrane-free system. Proc Natl Acad Sci 103, 4906–4911.

Higgs HN, Pollard TD (1999). Regulation of actin polymerization by Arp2/3 complex and WASp/Scar proteins. J Biol Chem 274, 32531–32534.

Ideses Y, Brill-Karniely Y, Haviv L, Ben-Shaul A, Bernheim-Groswasser A (2008). Arp2/3 branched actin network mediates filopodia-like bundles formation in vitro. PLoS One 3, e3297.

Kadzik RS, Homa KE, Kovar DR (2020). F-Actin cytoskeleton network self-organization through competition and cooperation. Annu Rev Cell Dev Biol 36, 35–60.

Knudsen KA, Soler AP, Johnson KR, Wheelock MJ (1995). Interaction of alpha-actinin with the cadherin/catenin cell-cell adhesion complex via alpha-catenin. J Cell Biol 130, 67–77.

Lipowsky R (2014). Coupling of bending and stretching deformations in vesicle membranes. Adv Colloid Interface Sci 208, 14–24.

Litschel T, Kelley CF, Holz D, Koudehi MA, Vogel SK, Burbaum L, Mizuno N, Vavylonis D, Schwille P (2021). Reconstitution of contractile actomyosin rings in vesicles. Nat Commun 12, 1–10.

Liu AP, Fletcher DA (2006). Actin polymerization serves as a membrane domain switch in model lipid bilayers. Biophys J 91, 4064–4070.

Liu AP, Richmond DL, Maibaum L, Pronk S, Geissler PL, Fletcher DA (2008). Membrane-induced bundling of actin filaments. Nat Phys 4, 789–793.

Machesky LM, Li A (2010). Fascin: Invasive filopodia promoting metastasis. Commun Integr Biol 3, 263–270.

Maciver SK, Wachsstock DH, Schwarz WH, Pollard TD (1991). The actin filament severing protein actophorin promotes the formation of rigid bundles of actin filaments crosslinked with alpha-actinin. J Cell Biol 115, 1621–1628.

Mullins RD, Heuser JA, Pollard TD (1998). The interaction of Arp2/3 complex with actin: nucleation, high affinity pointed end capping, and formation of branching networks of filaments. Proc Natl Acad Sci 95, 6181–6186.

Otey CA, Pavalko FM, Burridge K (1990). An interaction between alpha-actinin and the beta 1 integrin subunit in vitro. J Cell Biol 111, 721–729.

Pardee JD, Aspudich J (1982). [18]Purification of muscle actin. Methods Enzymol 85, 164–181.

Pettersen EF, Goddard TD, Huang CC, Couch GS, Greenblatt DM, Meng EC, Ferrin TE (2004). UCSF Chimera—a visualization system for exploratory research and analysis. J Comput Chem 25, 1605–1612.

Pollard TD (2007). Regulation of actin filament assembly by Arp2/3 complex and formins. Annu Rev Biophys Biomol Struct 36, 451–477.

Pollard TD, Beltzner CC (2002). Structure and function of the Arp2/3 complex. Curr Opin Struct Biol 12, 768–774.

Pontani L-L, Van der Gucht J, Salbreux G, Heuvingh J, Joanny J-F, Sykes C (2009). Reconstitution of an actin cortex inside a liposome. Biophys J 96, 192–198.

Robinson RC, Turbedsky K, Kaiser DA, Marchand J-B, Higgs HN, Choe S, Pollard TD (2001). Crystal structure of Arp2/3 complex. Science (80-) 294, 1679–1684.

Schafer DA (2002). Coupling actin dynamics and membrane dynamics during endocytosis. Curr Opin Cell Biol 14, 76–81.

Schindelin J, Arganda-Carreras I, Frise E, Kaynig V, Longair M, Pietzsch T, Preibisch S, Rueden C, Saalfeld S, Schmid B (2012). Fiji: an open-source platform for biological-image analysis. Nat Methods 9, 676–682.

Schmidt A, Hall MN (1998). Signaling to the actin cytoskeleton. Annu Rev Cell Dev Biol 14, 305–338.

Schneider CA, Rasband WS, Eliceiri KW (2012). NIH Image to ImageJ: 25 years of image analysis. Nat Methods 9, 671–675.

Simon C, Kusters R, Caorsi V, Allard A, Abou-Ghali M, Manzi J, Di Cicco A, Lévy D, Lenz M, Joanny J-F (2019). Actin dynamics drive cell-like membrane deformation. Nat Phys 15, 602–609.

Svitkina TM, Bulanova EA, Chaga OY, Vignjevic DM, Kojima S, Vasiliev JM, Borisy GG (2003). Mechanism of filopodia initiation by reorganization of a dendritic network. J Cell Biol 160, 409–421.

Tan TH, Malik-Garbi M, Abu-Shah E, Li J, Sharma A, MacKintosh FC, Keren K, Schmidt CF, Fakhri N (2018). Self-organized stress patterns drive state transitions in actin cortices. Sci Adv 4, eaar2847.

Tsai F-C, Koenderink GH (2015). Shape control of lipid bilayer membranes by confined actin bundles. Soft Matter 11, 8834–8847.

Vignjevic D, Kojima S, Aratyn Y, Danciu O, Svitkina T, Borisy GG (2006). Role of fascin in filopodial protrusion. J Cell Biol 174, 863–875.

Vignjevic D, Yarar D, Welch MD, Peloquin J, Svitkina T, Borisy GG (2003). Formation of filopodia-like bundles in vitro from a dendritic network. J Cell Biol 160, 951–962.

Weaver AM, Heuser JE, Karginov AV, Lee W, Parsons JT, Cooper JA (2002). Interaction of cortactin and N-WASp with Arp2/3 complex. Curr Biol 12, 1270–1278.

Welch MD (1999). The world according to Arp: regulation of actin nucleation by the Arp2/3 complex. Trends Cell Biol 9, 423–427.

Xu T, Vavylonis D, Huang X (2014). 3D actin network centerline extraction with multiple active contours. Med Image Anal 18, 272–284.

Xu T, Vavylonis D, Tsai F-C, Koenderink GH, Nie W, Yusuf E, Lee I-J, Wu J-Q, Huang X (2015). SOAX: a software for quantification of 3D biopolymer networks. Sci Rep 5, 1–10.